Volume 501 - 39th International Cosmic Ray Conference (ICRC2025) - Cosmic-Ray Indirect

Monitoring and Performance of AugerPrime

The Pierre Auger Collaboration, A. Abdul Halim, P. Abreu, M. Aglietta, I. Allekotte, K. Almeida Cheminant, et al. (click to show)

**: corresponding author*

Full text: pdf

Pre-published on: September 23, 2025
Published on: December 30, 2025

Abstract

The upgrade of Pierre Auger Observatory, AugerPrime, is a multi-hybrid system designed to improve the sensitivity and precision of ultra-high-energy cosmic ray measurements. It includes scintillator detectors positioned both atop the enhanced Water-Cherenkov detectors and buried nearby for direct muon measurements, along with radio and fluorescence detectors. In this contribution, we present an overview of the monitoring tools developed for all the components of AugerPrime, focusing on real-time performance assessment and long-term stability metrics. By continuously tracking key parameters, we can identify potential issues early, enabling timely interventions and improving overall data quality. These strategies are crucial for maintaining the long-term reliability of the measurements taken at the Auger Observatory and providing high-quality data for cosmic ray research in the coming decades.

DOI: https://doi.org/10.22323/1.501.0176

PROCEEDINGS OF SCIENCE

Monitoring and performance of AugerPrime

Belén Andrada[a,*] **for the Pierre Auger Collaboration**[b]

[a] *Instituto de Tecnología y Detección en Astropartículas (CNEA, CONICET, UNSAM), Buenos Aires, Argentina*

[b] *Observatorio Pierre Auger, Av. San Martín Norte 304, 5613 Malargüe, Argentina*

Full author list: https://www.auger.org/archive/authors_icrc_2025.html

E-mail: spokespersons@auger.org

The upgrade of Pierre Auger Observatory, AugerPrime, is a multi-hybrid system designed to improve the sensitivity and precision of ultra-high-energy cosmic ray measurements. It includes scintillator detectors positioned both atop the enhanced Water-Cherenkov detectors and buried nearby for direct muon measurements, along with radio and fluorescence detectors. In this contribution, we present an overview of the monitoring tools developed for all the components of AugerPrime, focusing on real-time performance assessment and long-term stability metrics. By continuously tracking key parameters, we can identify potential issues early, enabling timely interventions and improving overall data quality. These strategies are crucial for maintaining the long-term reliability of the measurements taken at the Auger Observatory and providing high-quality data for cosmic ray research in the coming decades.

39th International Cosmic Ray Conference (ICRC2025)
15–24 July 2025
Geneva, Switzerland

*Speaker

PoS(ICRC2025)176

1. The AugerPrime Surface Detector

The study of ultra-high-energy cosmic rays (UHECRs), with energies exceeding 10^{17} eV, remains one of the most compelling open questions in astroparticle physics. Key challenges include understanding their origin, acceleration mechanisms, and mass composition. The Pierre Auger Observatory was designed to address these questions by combining a large surface detector array with fluorescence telescopes, enabling the hybrid observation of extensive air showers over a wide energy range.

The Pierre Auger Observatory is located in Malargüe, Argentina, and comprises over 1660 surface detector stations arranged in triangular grids with spacings of 1500 m, 750 m, 433 m (called SD-1500, SD-750, and SD-433 respectively) and, covering a total area of approximately 3000 km^2 [1]. The surface array is complemented by 27 fluorescence telescopes installed at four peripheral buildings, as can be seen in the top-left panel of Fig. 1. While the denser sub-arrays enable low-energy event reconstruction, the fluorescence detector overlooks the atmosphere above the surface detector area to observe the longitudinal development of air showers and provides both mass-sensitive observables and a model-independent energy reconstruction.

During its first phase of operation (Phase I), the Observatory recorded high-quality data that led to significant advances, including precise measurements of the UHECR energy spectrum, constraints on photon and neutrino fluxes, and composition-sensitive observables [2]. These results suggest that the primary mass composition varies with energy while highlighting persistent uncertainties in hadronic interaction models at the highest energies.

To address these challenges and enhance composition sensitivity, the Auger Observatory has undergone a major upgrade known as AugerPrime [3]. As part of this upgrade, each Water-Cherenkov Detector (WCD) that is part of the surface array has been equipped with a small photomultiplier tube (SPMT) to extend its dynamic range and improve signal reconstruction near the shower core. In addition, the original electronics have been replaced by the Upgraded Unified Board (UUB), a new data acquisition system that digitizes signals from all detectors at 120 MHz with 12-bit resolution [4]. The UUB provides improved timing, triggering, and calibration functionality, ensuring compatibility with Phase I data while supporting the new AugerPrime instrumentation.

In addition to the WCD enhancements, each surface station now includes a Surface-Scintillator Detector (SSD) mounted above the WCD and a Radio Detector (RD) station installed on a mast, as can be seen in the right panel of Fig. 1. A dedicated Underground Muon Detector (UMD), almost fully deployed in the SD-750 and SD-433 regions (see bottom left panel of Fig. 1), complements these measurements by providing a direct view of the muonic component. Together, these additions allow for multi-component air shower reconstruction with improved sensitivity to mass composition.

A critical component of AugerPrime is the implementation of comprehensive monitoring systems across all detectors. These systems enable real-time tracking of key performance parameters, identification of potential issues, and long-term assessments of detector stability. In this work, we describe the monitoring infrastructure developed for each AugerPrime component and assess its performance during the initial years of Phase II data taking.

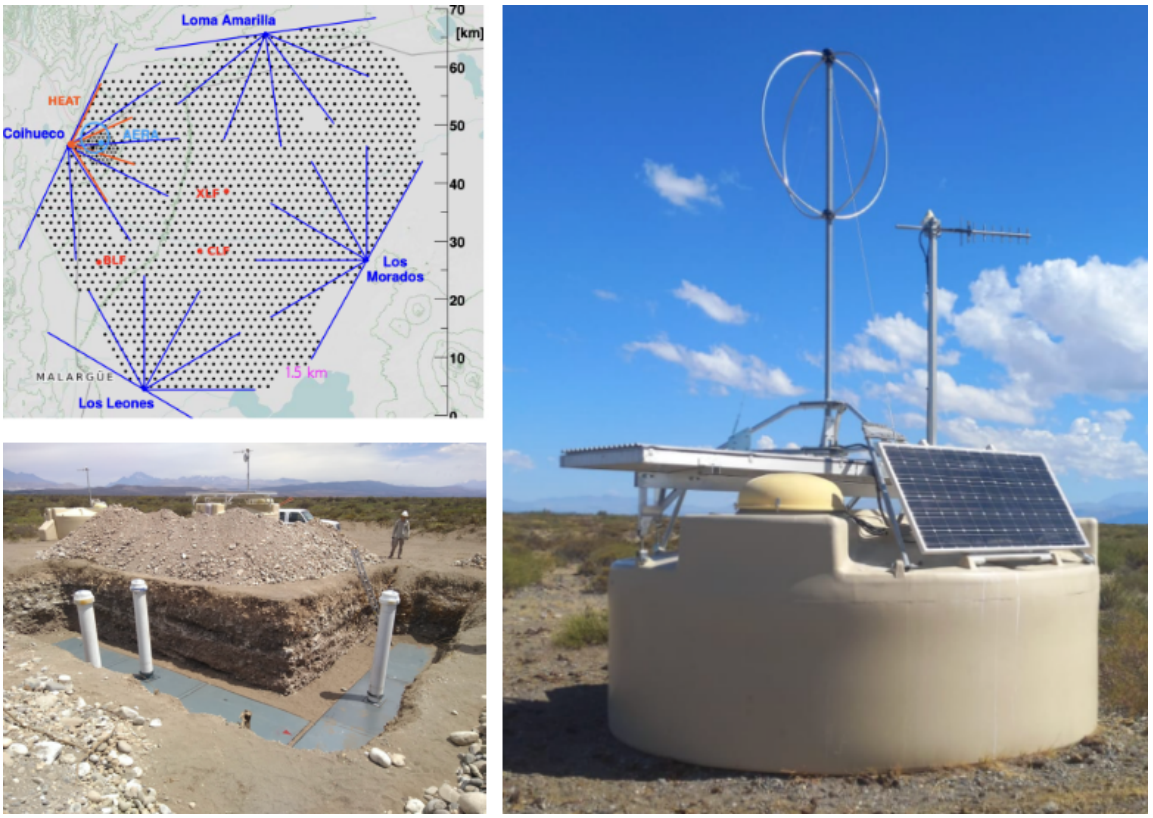

Figure 1: Top-left: layout of the Pierre Auger Observatory. Black dots represent surface detector stations and blue lines indicate the approximate field of view of the fluorescence telescopes in its four sites. The SD-750 and SD-433 arrays are located near the Coihueco site. Bottom-left: Underground Muon Detector station under deployment. Right: upgraded Water-Cherenkov detector, with a Scintillator detector and a Radio antenna.

2. Water-Cherenkov Detectors

The Water-Cherenkov Detectors form the core of the Surface Detector array and have operated reliably since the beginning of Phase I. Each WCD consists of a cylindrical tank filled with 12 000 l of purified water, instrumented with three downward-facing large photomultiplier tubes (LPMTs) mounted at the top. These PMTs detect Cherenkov light from charged particles and provide signals over a wide dynamic range suitable for most shower geometries.

As already mentioned, as part of the AugerPrime upgrade, a fourth, small PMT was added to extend the dynamic range, and the original electronics were replaced by the Upgraded Unified Board. The SPMT allows accurate measurement of high particle densities near the shower axis, while the UUB provides enhanced digitization, timing, and calibration capabilities [3]. This extends the WCD dynamic range by more than an order of magnitude, from a few hundred VEM (vertical equivalent muon) with the large PMTs to nearly 20,000 VEM with the SPMT.

The stability of the WCD array is shown in Fig. 2, which presents the daily rate of high-quality events per active hexagon for the SD-1500, as an example. The indicated energy threshold is chosen to ensure full trigger efficiency. Blue triangles indicate Phase I data, and red circles correspond to Phase II data, while the open gray circles show the transition period between the two. Rates remain

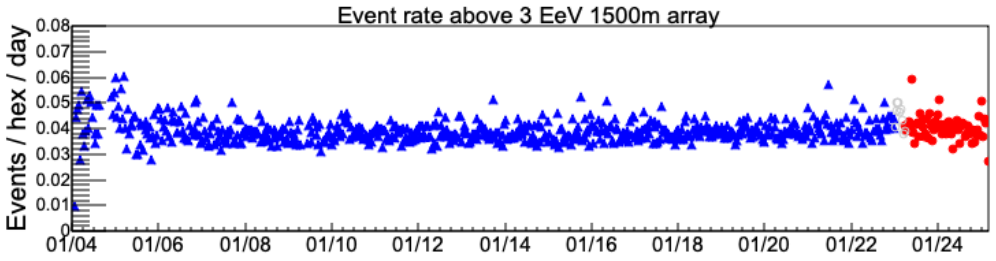

Figure 2: Daily rate of high-quality events per active hexagon for the SD-1500. The energy threshold ensures full trigger efficiency. Blue triangles indicate Phase I data, and red circles correspond to Phase II data, while the open gray circles show the transition period.

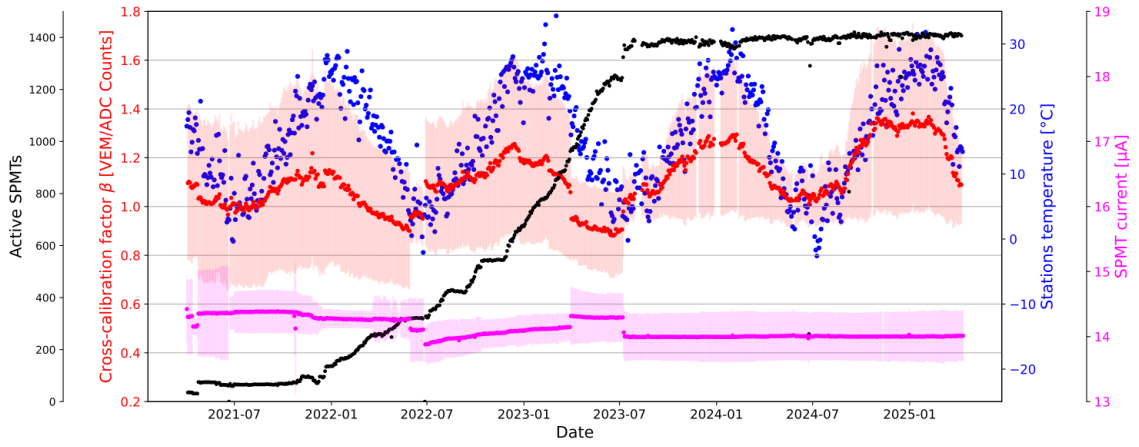

Figure 3: Evolution of SPMT-related parameters: number of active SPMTs (black), calibration factor β (red), station temperature (blue), and SPMT current (magenta), from 2021 to 2025.

stable over time, demonstrating consistent array performance during and after the deployment.

The SPMT, a 1-inch Hamamatsu R8619, cannot be directly calibrated with atmospheric muons due to its small photocathode area. A cross-calibration procedure is used instead, converting the integrated ADC signal to VEM via a linear relation, $S_{\mathrm{VEM}} = \beta\, Q_{\mathrm{ADC\ counts}}$, with a conversion factor β determined to better than 2.5 % [6].

The long-term evolution of SPMT-related parameters can be seen in Fig. 3. The number of active SPMTs (black) increases until mid-2023 as deployment progresses. The calibration factor β (red) shows a seasonal modulation of 8–10 %, consistent with the temperature dependence of SPMT gain. Temperature (blue), taken from sensors on the LPMTs, and SPMT current (magenta) reflect environmental trends and their effect on the hardware. In particular, the current stabilizes in mid-2023 following the activation of automatic high-voltage regulation.

The UUB digitizes waveforms from all detectors and provides unified acquisition across the upgraded Surface Detector [7]. It also maintains backward compatibility with Phase I triggers to support hybrid operation. Monitoring of voltage rails, temperature, and acquisition rates enables early issue detection and long-term stability tracking.

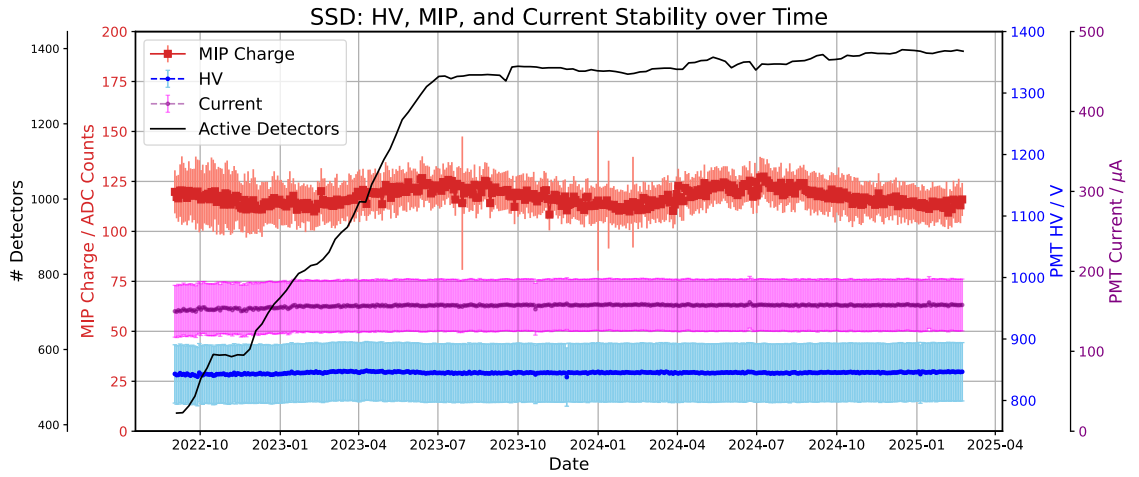

Figure 4: Daily averages of SSD MIP charge (red), PMT high voltage (blue), anode current (magenta), and the number of operational SSDs (black), grouped in 50-day intervals.

3. Surface Scintillator Detectors

Each Surface Scintillator Detector consists of two segmented plastic scintillator planes mounted above the WCD. Wavelength-shifting fibers collect scintillation light and guide it to a 1.5-inch Hamamatsu R9420 PMT. Unlike WCDs, which respond to both electromagnetic and muonic components, the SSDs are more sensitive to the electromagnetic component, enabling improved composition discrimination.

Calibration is primarily based on the response to atmospheric muons, which deposit a characteristic energy in the scintillator. This defines the minimum ionizing particle (MIP) signal, expressed in ADC counts, used as the reference unit for all signals [8].

The evolution of key monitoring parameters from late 2022 to early 2025 is shown in Fig. 4: MIP charge (red), PMT high voltage (blue), and anode current (magenta), along with the number of operational SSDs (black), averaged in 50-day intervals. The number of active detectors increases steadily during 2023 and stabilizes in mid-year, following installation completion and the start of Phase II data taking. High voltage and current remain stable, with no clear seasonal trend. In contrast, the MIP charge shows a 4–5 % seasonal modulation and diurnal variation (not shown here), attributed to the temperature dependence of PMT gain. Electronics temperatures remain stable, suggesting the gain is the primary source of variation [9].

4. Radio Detector

The Radio Detector measures coherent radio emission from extensive air showers in the 30–80 MHz band. Each RD station includes a dual-polarized Short Aperiodic Loaded Loop Antenna (SALLA) mounted above the WCD (see right panel of Fig. 1). The two orthogonal channels are aligned relative to the local geomagnetic field to maximize sensitivity to the dominant emission mechanisms. Signals are amplified, filtered, and digitized at 250 MHz with 12-bit resolution and are read out upon triggering by the associated WCD, ensuring precise timing across components.

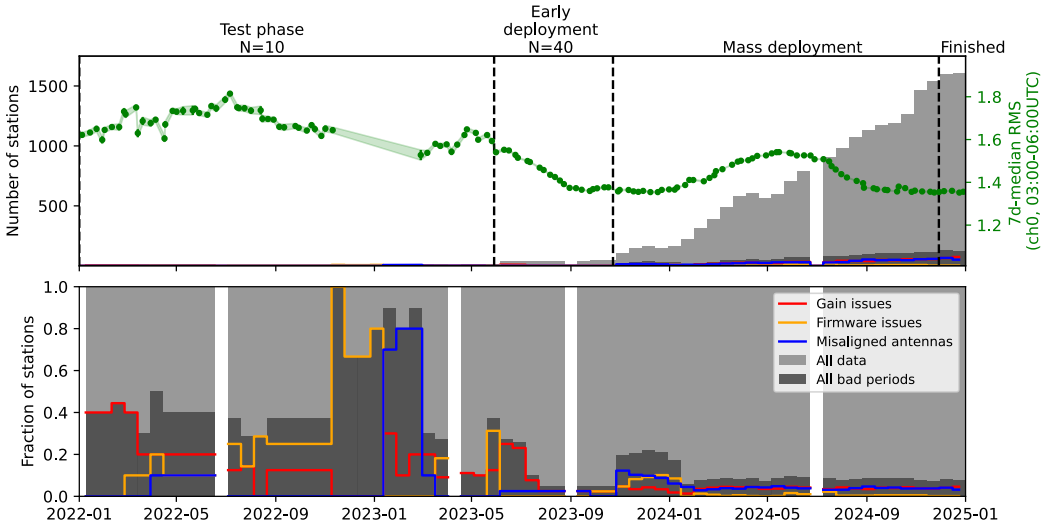

Figure 5: Number of operational RD stations from 2022 to 2025, with flagged periods (gray) marking quality issues. Vertical dashed lines indicate deployment milestones. Green markers in the top panel show the 7-day median RMS voltage, averaged over all active stations, calculated using data from 03:00–06:00 UTC only.

The number of operational RD stations over time can be observed in Fig. 5 as well as flagged periods where quality issues were detected. These include firmware errors, antenna misalignments, or gain instability, all identified through automated monitoring (see also [10]). The vertical lines mark transitions between deployment phases. Deployment began with a small number of stations in 2022, followed by mass installation between November 2023 and November 2024. By the end of 2024, nearly all stations reached stable performance.

An additional long-term observable is the average RMS voltage measured at each station, representing the total noise level in the signal band. About half of this RMS is due to diffuse galactic background emission, which is used as a calibration reference. The RMS increases during thunderstorms or transient events and is otherwise stable. Narrow-band radio-frequency interference (RFI) is filtered prior to RMS estimation to isolate broadband background variations [11]. To ensure consistent sky coverage throughout the year, RMS values shown in green on the top panel of Fig. 5 are computed only from data recorded between 03:00 and 06:00 UTC each day. This fixed time window reveals the seasonal modulation due to the galactic signal as the galaxy drifts across the night sky.

5. Underground Muon Detector

The Underground Muon Detector is installed in the SD-750 and SD-433 arrays to provide a direct measurement of the muonic component of extensive air showers. Each station includes three scintillator modules composed of 64 plastic scintillator strips, buried at a depth of 2.3 m (see bottom right panel of Fig. 1) and coupled to silicon photomultiplier (SiPM) arrays. Each SiPM detects light produced in a single strip via a wavelength-shifting fiber, enabling highly segmented detection of individual muons.

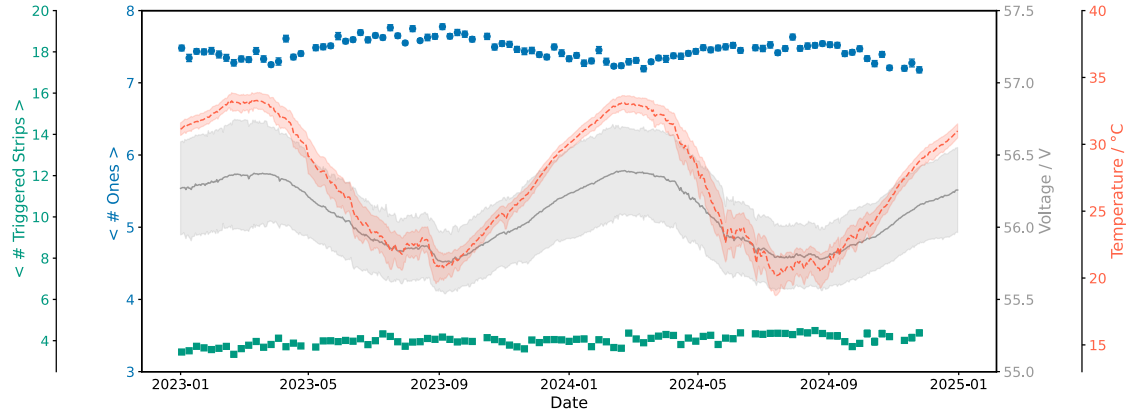

Figure 6: Daily averages of UMD monitoring parameters across all operational modules from 2023 to 2025: temperature measured at the high-voltage source (pink dashed line), applied voltage (gray solid line), average number of ones per trace (blue circles), and the average number of triggered strips per event with muon-like pattern (green squares).

The UMD operates in binary mode [13], where each strip is read out at 320 MHz and a digital "1" (one) is recorded whenever the signal exceeds a predefined threshold. This approach provides compact data with precise time resolution and robust noise suppression. Muon candidates are identified using a muon-like pattern, defined as at least four consecutive "1" bits in the binary trace (i.e., a pattern such as 1111) in the digitized trace. This pattern reflects the typical time structure of a muon signal and is used to count activated strips per event.

The long-term evolution of key monitoring observables for the UMD is presented in Fig. 6. These include the temperature measured at the high-voltage (HV) source (red dashed line), the applied HV (gray solid line), the average number of ones per trace (blue circles), and the average number of activated strips with a muon-like pattern per event (green squares). All variables are averaged over all operational modules in the array. A seasonal trend is observed in both temperature and voltage, as expected from the environmental modulation at the site. The HV source includes an internal temperature sensor and automatically adjusts the applied voltage to compensate for temperature-dependent shifts in the SiPM breakdown voltage. As the temperature decreases, the breakdown voltage of the SiPMs drops, increasing the overvoltage and, consequently, the gain. This results in larger signal amplitudes, effectively lowering the relative threshold and increasing the number of samples above the threshold. The resulting anticorrelation between temperature and the number of ones is clearly visible.

Despite the variations in gain and trace width, the average number of triggered strips per event remains stable over time. This confirms that the muon pattern recognition and event-level response are not significantly affected by temperature fluctuations or gain drift, highlighting the robustness of the binary mode and the effectiveness of the temperature compensation system. A gradual decrease in the number of ones is observed, corresponding to an average reduction of about 0.7 % per year [12]. This effect may reflect aging in the scintillators, SiPMs, or associated electronics and will continue to be monitored in future stability studies.

6. Conclusions

The AugerPrime upgrade has been successfully implemented across the Surface Detector array, with all components now integrated into a unified and modern data acquisition system. The deployment of new instrumentation— including SPMTs, SSDs, RDs, and UMDs—alongside the Upgraded Unified Board has significantly expanded the detector capabilities and maintained full compatibility with Phase I data.

In this contribution, we presented the monitoring infrastructure developed for each component and assessed its performance during the initial years of Phase II. The Water-Cherenkov Detectors exhibit stable operation and extended dynamic range. The Surface Scintillator Detectors maintain consistent calibration with well-understood seasonal variations. The Radio Detectors demonstrate reliable deployment and continuous background monitoring. The Underground Muon Detectors show stable response in binary mode, with robust muon pattern recognition and only minor aging effects observed.

Continuous monitoring of calibration parameters, environmental dependencies, and detector uptime is essential for ensuring high-quality data over the long term. These tools are key to maintaining the stability of the upgraded array and will support future performance studies and physics analyses throughout Phase II.

References

[1] A. Aab *et al.* [Pierre Auger Coll], Nucl. Instrum. Meth. A 798 (2015), 172-213

[2] D. Boncioli *et al.* [Pierre Auger Coll.], PoS(UHECR2024)027

[3] A. Castellina *et al.* [Pierre Auger Coll.], EPJ Web of Conferences 210, 06002 (2019)

[4] A. Abdul Halim *et al.*, JINST 18 (2023) P10016

[5] M. Buscemi *et al.*, JINST 15 (2020) P07011

[6] G. A. Anastasi *et al.* [Pierre Auger Coll.], PoS(ICRC2023)343

[7] M. Bohacova *et al.* [Pierre Auger Coll.], this proceedings

[8] P. Filip *et al.* [Pierre Auger Coll.], PoS(UHECR2024)085

[9] M. Conte *et al.* [Pierre Auger Coll.], this proceedings

[10] B. Pont *et al.* [Pierre Auger Coll.], this proceedings

[11] T. Fodran *et al.* [Pierre Auger Coll.], PoS(ARENA2022)425

[12] J. de Jesús *et al.* [Pierre Auger Coll.], PoS(ICRC2023)267

[13] J. de Jesús *et al.* [Pierre Auger Coll.], PoS(UHECR2024)077

The Pierre Auger Collaboration

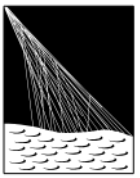

A. Abdul Halim[13], P. Abreu[70], M. Aglietta[53,51], I. Allekotte[1], K. Almeida Cheminant[78,77], A. Almela[7,12], R. Aloisio[44,45], J. Alvarez-Muñiz[76], A. Ambrosone[44], J. Ammerman Yebra[76], G.A. Anastasi[57,46], L. Anchordoqui[83], B. Andrada[7], L. Andrade Dourado[44,45], S. Andringa[70], L. Apollonio[58,48], C. Aramo[49], E. Arnone[62,51], J.C. Arteaga Velázquez[66], P. Assis[70], G. Avila[11], E. Avocone[56,45], A. Bakalova[31], F. Barbato[44,45], A. Bartz Mocellin[82], J.A. Bellido[13], C. Berat[35], M.E. Bertaina[62,51], M. Bianciotto[62,51], P.L. Biermann[a], V. Binet[5], K. Bismark[38,7], T. Bister[77,78], J. Biteau[36,i], J. Blazek[31], J. Blümer[40], M. Boháčová[31], D. Boncioli[56,45], C. Bonifazi[8], L. Bonneau Arbeletche[22], N. Borodai[68], J. Brack[f], P.G. Brichetto Orchera[7,40], F.L. Briechle[41], A. Bueno[75], S. Buitink[15], M. Buscemi[46,57], M. Büsken[38,7], A. Bwembya[77,78], K.S. Caballero-Mora[65], S. Cabana-Freire[76], L. Caccianiga[58,48], F. Campuzano[6], J. Caraça-Valente[82], R. Caruso[57,46], A. Castellina[53,51], F. Catalani[19], G. Cataldi[47], L. Cazon[76], M. Cerda[10], B. Čermáková[40], A. Cermenati[44,45], J.A. Chinellato[22], J. Chudoba[31], L. Chytka[32], R.W. Clay[13], A.C. Cobos Cerutti[6], R. Colalillo[59,49], R. Conceição[70], G. Consolati[48,54], M. Conte[55,47], F. Convenga[44,45], D. Correia dos Santos[27], P.J. Costa[70], C.E. Covault[81], M. Cristinziani[43], C.S. Cruz Sanchez[3], S. Dasso[4,2], K. Daumiller[40], B.R. Dawson[13], R.M. de Almeida[27], E.-T. de Boone[43], B. de Errico[27], J. de Jesús[7], S.J. de Jong[77,78], J.R.T. de Mello Neto[27], I. De Mitri[44,45], J. de Oliveira[18], D. de Oliveira Franco[42], F. de Palma[55,47], V. de Souza[20], E. De Vito[55,47], A. Del Popolo[57,46], O. Deligny[33], N. Denner[31], L. Deval[53,51], A. di Matteo[51], C. Dobrigkeit[22], J.C. D'Olivo[67], L.M. Domingues Mendes[16,70], Q. Dorosti[43], J.C. dos Anjos[16], R.C. dos Anjos[26], J. Ebr[31], F. Ellwanger[40], R. Engel[38,40], I. Epicoco[55,47], M. Erdmann[41], A. Etchegoyen[7,12], C. Evoli[44,45], H. Falcke[77,79,78], G. Farrar[85], A.C. Fauth[22], T. Fehler[43], F. Feldbusch[39], A. Fernandes[70], M. Fernandez[14], B. Fick[84], J.M. Figueira[7], P. Filip[38,7], A. Filipčič[74,73], T. Fitoussi[40], B. Flaggs[87], T. Fodran[77], A. Franco[47], M. Freitas[70], T. Fujii[86,h], A. Fuster[7,12], C. Galea[77], B. García[6], C. Gaudu[37], P.L. Ghia[33], U. Giaccari[47], F. Gobbi[10], F. Gollan[7], G. Golup[1], M. Gómez Berisso[1], P.F. Gómez Vitale[11], J.P. Gongora[11], J.M. González[1], N. González[7], D. Góra[68], A. Gorgi[53,51], M. Gottowik[40], F. Guarino[59,49], G.P. Guedes[23], L. Gülzow[40], S. Hahn[38], P. Hamal[31], M.R. Hampel[7], P. Hansen[3], V.M. Harvey[13], A. Haungs[40], T. Hebbeker[41], C. Hojvat[d], J.R. Hörandel[77,78], P. Horvath[32], M. Hrabovský[32], T. Huege[40,15], A. Insolia[57,46], P.G. Isar[72], M. Ismaiel[77,78], P. Janecek[31], V. Jilek[31], K.-H. Kampert[37], B. Keilhauer[40], A. Khakurdikar[77], V.V. Kizakke Covilakam[7,40], H.O. Klages[40], M. Kleifges[39], J. Köhler[40], F. Krieger[41], M. Kubatova[31], N. Kunka[39], B.L. Lago[17], N. Langner[41], N. Leal[7], M.A. Leigui de Oliveira[25], Y. Lema-Capeans[76], A. Letessier-Selvon[34], I. Lhenry-Yvon[33], L. Lopes[70], J.P. Lundquist[73], M. Mallamaci[60,46], D. Mandat[31], P. Mantsch[d], F.M. Mariani[58,48], A.G. Mariazzi[3], I.C. Mariş[14], G. Marsella[60,46], D. Martello[55,47], S. Martinelli[40,7], M.A. Martins[76], H.-J. Mathes[40], J. Matthews[g], G. Matthiae[61,50], E. Mayotte[82], S. Mayotte[82], P.O. Mazur[d], G. Medina-Tanco[67], J. Meinert[37], D. Melo[7], A. Menshikov[39], C. Merx[40], S. Michal[31], M.I. Micheletti[5], L. Miramonti[58,48], M. Mogarkar[68], S. Mollerach[1], F. Montanet[35], L. Morejon[37], K. Mulrey[77,78], R. Mussa[51], W.M. Namasaka[37], S. Negi[31], L. Nellen[67], K. Nguyen[84], G. Nicora[9], M. Niechciol[43], D. Nitz[84], D. Nosek[30], A. Novikov[87], V. Novotny[30], L. Nožka[32], A. Nucita[55,47], L.A. Núñez[29], J. Ochoa[7,40], C. Oliveira[20], L. Östman[31], M. Palatka[31], J. Pallotta[9], S. Panja[31], G. Parente[76], T. Paulsen[37], J. Pawlowsky[37], M. Pech[31], J. Pękala[68], R. Pelayo[64], V. Pelgrims[14], L.A.S. Pereira[24], E.E. Pereira Martins[38,7], C. Pérez Bertolli[7,40], L. Perrone[55,47], S. Petrera[44,45], C. Petrucci[56], T. Pierog[40], M. Pimenta[70], M. Platino[7], B. Pont[77], M. Pourmohammad Shahvar[60,46], P. Privitera[86], C. Priyadarshi[68], M. Prouza[31], K. Pytel[69], S. Querchfeld[37], J. Rautenberg[37], D. Ravignani[7], J.V. Reginatto Akim[22], A. Reuzki[41], J. Ridky[31], F. Riehn[76,j], M. Risse[43], V. Rizi[56,45], E. Rodriguez[7,40], G. Rodriguez Fernandez[50], J. Rodriguez Rojo[11], S. Rossoni[42], M. Roth[40], E. Roulet[1], A.C. Rovero[4], A. Saftoiu[71], M. Saharan[77], F. Salamida[56,45], H. Salazar[63], G. Salina[50], P. Sampathkumar[40], N. San Martin[82], J.D. Sanabria Gomez[29], F. Sánchez[7], E.M. Santos[21], E. Santos[31], F. Sarazin[82], R. Sarmento[70], R. Sato[11], P. Savina[44,45], V. Scherini[55,47], H. Schieler[40], M. Schimassek[33], M. Schimp[37], D. Schmidt[40], O. Scholten[15,b], H. Schoorlemmer[77,78], P. Schovánek[31], F.G. Schröder[87,40], J. Schulte[41], T. Schulz[31], S.J. Sciutto[3], M. Scornavacche[7], A. Sedoski[7], A. Segreto[52,46], S. Sehgal[37], S.U. Shivashankara[73], G. Sigl[42], K. Simkova[15,14], F. Simon[39], R. Šmída[86], P. Sommers[e], R. Squartini[10], M. Stadelmaier[40,48,58], S. Stanič[73], J. Stasielak[68], P. Stassi[35], S. Strähnz[38], M. Straub[41], T. Suomijärvi[36], A.D. Supanitsky[7], Z. Svozilikova[31], K. Syrokvas[30], Z. Szadkowski[69], F. Tairli[13], M. Tambone[59,49], A. Tapia[28], C. Taricco[62,51], C. Timmermans[78,77], O. Tkachenko[31], P. Tobiska[31], C.J. Todero Peixoto[19], B. Tomé[70], A. Travaini[10], P. Travnicek[31], M. Tueros[3], M. Unger[40], R. Uzeiroska[37], L. Vaclavek[32], M. Vacula[32], I. Vaiman[44,45], J.F. Valdés Galicia[67], L. Valore[59,49], P. van Dillen[77,78], E. Varela[63], V. Vašíčková[37], A. Vásquez-Ramírez[29], D. Veberič[40], I.D. Vergara Quispe[3], S. Verpoest[87], V. Verzi[50], J. Vicha[31], J. Vink[80], S. Vorobiov[73], J.B. Vuta[31], C. Watanabe[27], A.A. Watson[c], A. Weindl[40], M. Weitz[37], L. Wiencke[82], H. Wilczyński[68], B. Wundheiler[7], B. Yue[37], A. Yushkov[31], E. Zas[76], D. Zavrtanik[73,74], M. Zavrtanik[74,73]

[1] Centro Atómico Bariloche and Instituto Balseiro (CNEA-UNCuyo-CONICET), San Carlos de Bariloche, Argentina
[2] Departamento de Física and Departamento de Ciencias de la Atmósfera y los Océanos, FCEyN, Universidad de Buenos Aires and CONICET, Buenos Aires, Argentina
[3] IFLP, Universidad Nacional de La Plata and CONICET, La Plata, Argentina
[4] Instituto de Astronomía y Física del Espacio (IAFE, CONICET-UBA), Buenos Aires, Argentina
[5] Instituto de Física de Rosario (IFIR) – CONICET/U.N.R. and Facultad de Ciencias Bioquímicas y Farmacéuticas U.N.R., Rosario, Argentina
[6] Instituto de Tecnologías en Detección y Astropartículas (CNEA, CONICET, UNSAM), and Universidad Tecnológica Nacional – Facultad Regional Mendoza (CONICET/CNEA), Mendoza, Argentina
[7] Instituto de Tecnologías en Detección y Astropartículas (CNEA, CONICET, UNSAM), Buenos Aires, Argentina
[8] International Center of Advanced Studies and Instituto de Ciencias Físicas, ECyT-UNSAM and CONICET, Campus Miguelete – San Martín, Buenos Aires, Argentina
[9] Laboratorio Atmósfera – Departamento de Investigaciones en Láseres y sus Aplicaciones – UNIDEF (CITEDEF-CONICET), Argentina
[10] Observatorio Pierre Auger, Malargüe, Argentina
[11] Observatorio Pierre Auger and Comisión Nacional de Energía Atómica, Malargüe, Argentina
[12] Universidad Tecnológica Nacional – Facultad Regional Buenos Aires, Buenos Aires, Argentina
[13] University of Adelaide, Adelaide, S.A., Australia
[14] Université Libre de Bruxelles (ULB), Brussels, Belgium
[15] Vrije Universiteit Brussels, Brussels, Belgium
[16] Centro Brasileiro de Pesquisas Fisicas, Rio de Janeiro, RJ, Brazil
[17] Centro Federal de Educação Tecnológica Celso Suckow da Fonseca, Petropolis, Brazil
[18] Instituto Federal de Educação, Ciência e Tecnologia do Rio de Janeiro (IFRJ), Brazil
[19] Universidade de São Paulo, Escola de Engenharia de Lorena, Lorena, SP, Brazil
[20] Universidade de São Paulo, Instituto de Física de São Carlos, São Carlos, SP, Brazil
[21] Universidade de São Paulo, Instituto de Física, São Paulo, SP, Brazil
[22] Universidade Estadual de Campinas (UNICAMP), IFGW, Campinas, SP, Brazil
[23] Universidade Estadual de Feira de Santana, Feira de Santana, Brazil
[24] Universidade Federal de Campina Grande, Centro de Ciencias e Tecnologia, Campina Grande, Brazil
[25] Universidade Federal do ABC, Santo André, SP, Brazil
[26] Universidade Federal do Paraná, Setor Palotina, Palotina, Brazil
[27] Universidade Federal do Rio de Janeiro, Instituto de Física, Rio de Janeiro, RJ, Brazil
[28] Universidad de Medellín, Medellín, Colombia
[29] Universidad Industrial de Santander, Bucaramanga, Colombia
[30] Charles University, Faculty of Mathematics and Physics, Institute of Particle and Nuclear Physics, Prague, Czech Republic
[31] Institute of Physics of the Czech Academy of Sciences, Prague, Czech Republic
[32] Palacky University, Olomouc, Czech Republic
[33] CNRS/IN2P3, IJCLab, Université Paris-Saclay, Orsay, France
[34] Laboratoire de Physique Nucléaire et de Hautes Energies (LPNHE), Sorbonne Université, Université de Paris, CNRS-IN2P3, Paris, France
[35] Univ. Grenoble Alpes, CNRS, Grenoble Institute of Engineering Univ. Grenoble Alpes, LPSC-IN2P3, 38000 Grenoble, France
[36] Université Paris-Saclay, CNRS/IN2P3, IJCLab, Orsay, France
[37] Bergische Universität Wuppertal, Department of Physics, Wuppertal, Germany
[38] Karlsruhe Institute of Technology (KIT), Institute for Experimental Particle Physics, Karlsruhe, Germany
[39] Karlsruhe Institute of Technology (KIT), Institut für Prozessdatenverarbeitung und Elektronik, Karlsruhe, Germany
[40] Karlsruhe Institute of Technology (KIT), Institute for Astroparticle Physics, Karlsruhe, Germany
[41] RWTH Aachen University, III. Physikalisches Institut A, Aachen, Germany
[42] Universität Hamburg, II. Institut für Theoretische Physik, Hamburg, Germany
[43] Universität Siegen, Department Physik – Experimentelle Teilchenphysik, Siegen, Germany
[44] Gran Sasso Science Institute, L'Aquila, Italy
[45] INFN Laboratori Nazionali del Gran Sasso, Assergi (L'Aquila), Italy
[46] INFN, Sezione di Catania, Catania, Italy
[47] INFN, Sezione di Lecce, Lecce, Italy
[48] INFN, Sezione di Milano, Milano, Italy
[49] INFN, Sezione di Napoli, Napoli, Italy
[50] INFN, Sezione di Roma "Tor Vergata", Roma, Italy
[51] INFN, Sezione di Torino, Torino, Italy

PoS(ICRC2025)176

[52] Istituto di Astrofisica Spaziale e Fisica Cosmica di Palermo (INAF), Palermo, Italy
[53] Osservatorio Astrofisico di Torino (INAF), Torino, Italy
[54] Politecnico di Milano, Dipartimento di Scienze e Tecnologie Aerospaziali , Milano, Italy
[55] Università del Salento, Dipartimento di Matematica e Fisica "E. De Giorgi", Lecce, Italy
[56] Università dell'Aquila, Dipartimento di Scienze Fisiche e Chimiche, L'Aquila, Italy
[57] Università di Catania, Dipartimento di Fisica e Astronomia "Ettore Majorana", Catania, Italy
[58] Università di Milano, Dipartimento di Fisica, Milano, Italy
[59] Università di Napoli "Federico II", Dipartimento di Fisica "Ettore Pancini", Napoli, Italy
[60] Università di Palermo, Dipartimento di Fisica e Chimica "E. Segrè", Palermo, Italy
[61] Università di Roma "Tor Vergata", Dipartimento di Fisica, Roma, Italy
[62] Università Torino, Dipartimento di Fisica, Torino, Italy
[63] Benemérita Universidad Autónoma de Puebla, Puebla, México
[64] Unidad Profesional Interdisciplinaria en Ingeniería y Tecnologías Avanzadas del Instituto Politécnico Nacional (UPIITA-IPN), México, D.F., México
[65] Universidad Autónoma de Chiapas, Tuxtla Gutiérrez, Chiapas, México
[66] Universidad Michoacana de San Nicolás de Hidalgo, Morelia, Michoacán, México
[67] Universidad Nacional Autónoma de México, México, D.F., México
[68] Institute of Nuclear Physics PAN, Krakow, Poland
[69] University of Łódź, Faculty of High-Energy Astrophysics,Łódź, Poland
[70] Laboratório de Instrumentação e Física Experimental de Partículas – LIP and Instituto Superior Técnico – IST, Universidade de Lisboa – UL, Lisboa, Portugal
[71] "Horia Hulubei" National Institute for Physics and Nuclear Engineering, Bucharest-Magurele, Romania
[72] Institute of Space Science, Bucharest-Magurele, Romania
[73] Center for Astrophysics and Cosmology (CAC), University of Nova Gorica, Nova Gorica, Slovenia
[74] Experimental Particle Physics Department, J. Stefan Institute, Ljubljana, Slovenia
[75] Universidad de Granada and C.A.F.P.E., Granada, Spain
[76] Instituto Galego de Física de Altas Enerxías (IGFAE), Universidade de Santiago de Compostela, Santiago de Compostela, Spain
[77] IMAPP, Radboud University Nijmegen, Nijmegen, The Netherlands
[78] Nationaal Instituut voor Kernfysica en Hoge Energie Fysica (NIKHEF), Science Park, Amsterdam, The Netherlands
[79] Stichting Astronomisch Onderzoek in Nederland (ASTRON), Dwingeloo, The Netherlands
[80] Universiteit van Amsterdam, Faculty of Science, Amsterdam, The Netherlands
[81] Case Western Reserve University, Cleveland, OH, USA
[82] Colorado School of Mines, Golden, CO, USA
[83] Department of Physics and Astronomy, Lehman College, City University of New York, Bronx, NY, USA
[84] Michigan Technological University, Houghton, MI, USA
[85] New York University, New York, NY, USA
[86] University of Chicago, Enrico Fermi Institute, Chicago, IL, USA
[87] University of Delaware, Department of Physics and Astronomy, Bartol Research Institute, Newark, DE, USA

---

[a] Max-Planck-Institut für Radioastronomie, Bonn, Germany
[b] also at Kapteyn Institute, University of Groningen, Groningen, The Netherlands
[c] School of Physics and Astronomy, University of Leeds, Leeds, United Kingdom
[d] Fermi National Accelerator Laboratory, Fermilab, Batavia, IL, USA
[e] Pennsylvania State University, University Park, PA, USA
[f] Colorado State University, Fort Collins, CO, USA
[g] Louisiana State University, Baton Rouge, LA, USA
[h] now at Graduate School of Science, Osaka Metropolitan University, Osaka, Japan
[i] Institut universitaire de France (IUF), France
[j] now at Technische Universität Dortmund and Ruhr-Universität Bochum, Dortmund and Bochum, Germany

Acknowledgments

The successful installation, commissioning, and operation of the Pierre Auger Observatory would not have been possible without the strong commitment and effort from the technical and administrative staff in Malargüe. We are very grateful to the following agencies and organizations for financial support:

Argentina – Comisión Nacional de Energía Atómica; Agencia Nacional de Promoción Científica y Tecnológica (ANPCyT); Consejo Nacional de Investigaciones Científicas y Técnicas (CONICET); Gobierno de la Provincia de Mendoza; Municipalidad de Malargüe; NDM Holdings and Valle Las Leñas; in gratitude for their continuing cooperation over land

access; Australia – the Australian Research Council; Belgium – Fonds de la Recherche Scientifique (FNRS); Research Foundation Flanders (FWO), Marie Curie Action of the European Union Grant No. 101107047; Brazil – Conselho Nacional de Desenvolvimento Científico e Tecnológico (CNPq); Financiadora de Estudos e Projetos (FINEP); Fundação de Amparo à Pesquisa do Estado de Rio de Janeiro (FAPERJ); São Paulo Research Foundation (FAPESP) Grants No. 2019/10151-2, No. 2010/07359-6 and No. 1999/05404-3; Ministério da Ciência, Tecnologia, Inovações e Comunicações (MCTIC); Czech Republic – GACR 24-13049S, CAS LQ100102401, MEYS LM2023032, CZ.02.1.01/0.0/0.0/16_013/0001402, CZ.02.1.01/0.0/0.0/18_046/0016010 and CZ.02.1.01/0.0/0.0/17_049/0008422 and CZ.02.01.01/00/22_008/0004632; France – Centre de Calcul IN2P3/CNRS; Centre National de la Recherche Scientifique (CNRS); Conseil Régional Ile-de-France; Département Physique Nucléaire et Corpusculaire (PNC-IN2P3/CNRS); Département Sciences de l'Univers (SDU-INSU/CNRS); Institut Lagrange de Paris (ILP) Grant No. LABEX ANR-10-LABX-63 within the Investissements d'Avenir Programme Grant No. ANR-11-IDEX-0004-02; Germany – Bundesministerium für Bildung und Forschung (BMBF); Deutsche Forschungsgemeinschaft (DFG); Finanzministerium Baden-Württemberg; Helmholtz Alliance for Astroparticle Physics (HAP); Helmholtz-Gemeinschaft Deutscher Forschungszentren (HGF); Ministerium für Kultur und Wissenschaft des Landes Nordrhein-Westfalen; Ministerium für Wissenschaft, Forschung und Kunst des Landes Baden-Württemberg; Italy – Istituto Nazionale di Fisica Nucleare (INFN); Istituto Nazionale di Astrofisica (INAF); Ministero dell'Università e della Ricerca (MUR); CETEMPS Center of Excellence; Ministero degli Affari Esteri (MAE), ICSC Centro Nazionale di Ricerca in High Performance Computing, Big Data and Quantum Computing, funded by European Union NextGenerationEU, reference code CN_00000013; México – Consejo Nacional de Ciencia y Tecnología (CONACYT) No. 167733; Universidad Nacional Autónoma de México (UNAM); PAPIIT DGAPA-UNAM; The Netherlands – Ministry of Education, Culture and Science; Netherlands Organisation for Scientific Research (NWO); Dutch national e-infrastructure with the support of SURF Cooperative; Poland – Ministry of Education and Science, grants No. DIR/WK/2018/11 and 2022/WK/12; National Science Centre, grants No. 2016/22/M/ST9/00198, 2016/23/B/ST9/01635, 2020/39/B/ST9/01398, and 2022/45/B/ST9/02163; Portugal – Portuguese national funds and FEDER funds within Programa Operacional Factores de Competitividade through Fundação para a Ciência e a Tecnologia (COMPETE); Romania – Ministry of Research, Innovation and Digitization, CNCS-UEFISCDI, contract no. 30N/2023 under Romanian National Core Program LAPLAS VII, grant no. PN 23 21 01 02 and project number PN-III-P1-1.1-TE-2021-0924/TE57/2022, within PNCDI III; Slovenia – Slovenian Research Agency, grants P1-0031, P1-0385, I0-0033, N1-0111; Spain – Ministerio de Ciencia e Innovación/Agencia Estatal de Investigación (PID2019-105544GB-I00, PID2022-140510NB-I00 and RYC2019-027017-I), Xunta de Galicia (CIGUS Network of Research Centers, Consolidación 2021 GRC GI-2033, ED431C-2021/22 and ED431F-2022/15), Junta de Andalucía (SOMM17/6104/UGR and P18-FR-4314), and the European Union (Marie Sklodowska-Curie 101065027 and ERDF); USA – Department of Energy, Contracts No. DE-AC02-07CH11359, No. DE-FR02-04ER41300, No. DE-FG02-99ER41107 and No. DE-SC0011689; National Science Foundation, Grant No. 0450696, and NSF-2013199; The Grainger Foundation; Marie Curie-IRSES/EPLANET; European Particle Physics Latin American Network; and UNESCO.